THE ASTROPHYSICAL JOURNAL, 435:469–481, 1994 November 1

A THERMAL/NONTHERMAL MODEL FOR SOLAR HARD X-RAY BURSTS

STEPHEN G. BENKA[1]
E. O. Hulburt Center for Space Research, Naval Research Laboratory, Code 7675B, Washington, DC 20375-5352
AND
GORDON D. HOLMAN
Laboratory for Astronomy and Solar Physics, NASA/Goddard Space Flight Center, Code 682.1, Greenbelt, MD 20771
Received 1993 September 27; accepted 1994 May 5

ABSTRACT

A formalism is developed for analyzing high-resolution hard X-ray spectra, incorporating the coexistence of thermal and nonthermal bremsstrahlung. The two processes are physically linked by the presence of electric currents, which both heat the surrounding plasma via Joule dissipation and accelerate electrons via the runaway process. We use this formalism to analyze the flare of 1980 June 27 and find that both the gradual and spike components of the hard X-ray emission are consistent with runaway acceleration. We also find that significant heating is observed only in the gradual component. The electric field is always sub-Dreicer, the maximum total potential drop in the acceleration region is found to be ~ 100 kV in two of the spikes, and the average accelerated electron flux is $\sim 10^{34}$ electrons s^{-1}. We argue that classical resistivity is a valid assumption for this event and find the density in the current channels ($\sim 10^{11}$ cm^{-3}) and a lower limit on the volume of the heated plasma. We find that the ratio of the electric field to the Dreicer field ($\epsilon = E/E_D$) varies systematically, whereas the value of E alone does not. We also find that the acceleration region fragmented into many current/return current pairs, and that the fragmentation varied systematically. We also discuss further implications of this model.

Subject headings: acceleration of particles — MHD — radiation mechanisms: nonthermal — radiation mechanisms: thermal — Sun: flares — Sun: X-rays, gamma rays

1. INTRODUCTION

The impulsive phase of solar flares is characterized by rapidly varying hard X-ray and microwave radiation, widely believed to result from "impulsive" energy release associated with the flare triggering mechanism. This energy release both heats the coronal plasma to temperatures in excess of 10^7 K, and accelerates prodigious numbers of electrons to energies in excess of 100 keV. The free energy which powers these events is almost certainly derived from nonpotential magnetic fields and their associated currents. The presence of currents in the solar atmosphere during flares provides a natural mechanism for both heating and acceleration to occur. Since the resistivity of the coronal plasma is finite, a macroscopic electric field must be present, $\boldsymbol{E} = \eta \boldsymbol{J}$, and Joule heating will take place at a rate of $\boldsymbol{J} \cdot \boldsymbol{E}$ ergs cm^{-3} s^{-1}. Concurrently, electrons whose momentum exceeds a critical momentum, p_{cr}, will be freely accelerated by the electric field, unhindered by collisions (e.g., Dreicer 1959; Heyvaerts 1981; Spicer 1982; Holman 1985; Tsuneta 1985). Since p_{cr} is typically only a few times the thermal momentum, p_{th}, these "runaway electrons" can constitute a significant fraction of the electrons present.

To date, the simultaneous primary heating and acceleration which must occur in the impulsive phase have not received a very balanced treatment. It has been implicitly assumed that one of these processes was completely dominant over the other. In retrospect, it is good that both views developed early (see Holman & Benka 1992 for a brief history), since the low-quality spectra (by today's standards) did not require more sophisticated treatment, and much has been learned from the interplay of these opposing viewpoints over the years (Tandberg-Hanssen & Emslie 1988; Dennis 1988; Dennis & Schwartz 1989).

Today, however, it is more difficult to justify these simple approaches. Since the first flight of a cooled, high-purity germanium detector and the discovery of a new superhot thermal component in a hard X-ray burst (Lin et al. 1981), it is apparent that neither heating alone nor acceleration alone can in general account for the observations, except for certain special events. The spectra of the 1980 June 27 event (Lin et al. 1981) clearly showed an emerging (superhot) thermal component at energies below ~ 40 keV in addition to nonthermal radiation at higher energies. Hamilton & Petrosian (1992) dispute the thermal nature of the low-energy component, but analysis of the data has shown a thermal interpretation is the likely one (Emslie, Coffey, & Schwartz 1989). This remains the only event observed with germanium detectors with their high energy resolution. The very large area of the detectors on NASA's *Compton Gamma-Ray Observatory* satellite, however, may make the detection of this additional thermal component routine (Schwartz et al. 1993).

In recent years the importance of *both* heating and acceleration has become more widely recognized. Böhme et al. (1977) proposed a two-component flare model with a core of nonthermal particles within a thermal halo. Shevgaonkar & Kundu (1985) required both thermal and nonthermal particles and invoked DC electric fields to explain microwave bursts. Holman (1985) studied simultaneous heating and acceleration in current sheets and found that a well-observed flare could be analyzed within this framework (Holman, Kundu, & Kane 1989). A similar study was performed by Tsuneta (1985), who considered the plasma density effects on the heating and acceleration in current threads. In another flare, Nitta, Kiplinger, &

[1] Current address: American Institute of Physics, One Physics Ellipse, College Park, MD 20740-3843.

Kai (1989) found precipitating nonthermal electrons as well as two thermal components ($T = 2.2$ and 7×10^7 K). Willson et al. (1990) studied two spatially and temporally separated components of one flare and concluded that one was thermal, the other nonthermal. Li & Emslie (1990) have investigated the secondary heating which must accompany the nonthermal model. Winglee et al. (1991) have studied particle simulations of concurrent electric field acceleration and wave/particle heating. Benka & Holman (1992) found that a hybrid thermal/nonthermal model could account for several previously unexplained features in high-resolution microwave spectra. All of these examples require both thermal and nonthermal processes.

There are several possible mechanisms which could provide simultaneous acceleration and heating, the simplest of which invokes the DC electric fields which are known to be present during flares. Holman & Benka (1992) presented a simple approach, using such fields, to model high-resolution hard X-ray spectra. To do this, they assumed a priori the existence of currents during a flare, with the attendant Joule dissipation and runaway acceleration being therefore physically coupled. The heated plasma emits thermal bremsstrahlung while the runaway electrons produce thick-target emission in the chromosphere. There are no spatial constraints, in the sense that the Joule-heated plasma and the thick target on which the accelerated electrons impinge need not be cospatial.

In this paper we present the details of this approach and reanalyze the 1980 June 27 event within this framework. We account for the physically distinct gradual and spike components of the emission, first noticed by Lin & Schwartz (1987), and find excellent agreement between the theory and the data. Specifically, the emission in the spikes is fully consistent with pure runaway acceleration, while both heating and acceleration are apparent in the underlying gradual component of the emission. We find that the electric fields are always sub-Dreicer and that classical resistivity is a valid assumption. We evaluate both the nonthermal and thermal energetics of this event, finding good agreement with Lin & Johns (1993) for the accelerated electrons.

In § 2 we obtain approximate electron distribution functions for both runaway and the "thermal" current within a current channel. In § 3, thick-target bremsstrahlung is calculated from the runaway distribution, as is thermal bremsstrahlung from a surrounding plasma at the current sheet temperature, and compared with the spectra observed for the 1980 June 27 flare. The time evolution of flare parameters is obtained. In § 4 we discuss our results and some further implications of this model.

2. CURRENT SHEET ELECTRON DISTRIBUTIONS

In order to calculate a hard X-ray spectrum, we must know the distribution function for the electrons which produce it. In this section we present our approximation to the distribution function for electrons within an external electric field of finite spatial extent. The two dominant competing processes in such a field are (i) collisions which tend to isotropize the distribution, and (ii) electric field acceleration which produces a nonthermal tail on the distribution, extending antiparallel to the direction of the field. Since the particle collision frequency is proportional to p^{-3}, the high-energy electrons are effectively collisionless and can be freely accelerated by the electric field. These are the runaway electrons. The lower energy electrons in the highly collisional regime serve mainly to heat the plasma through Joule dissipation. The separation between these two regimes occurs at the *critical momentum*, p_{cr}, at which the competing effects of collisions and unidirectional acceleration are just balanced, as found by Dreicer (1959). In § 2.1 we determine the runaway distribution function ($p > p_{cr}$) (eqs. [7]–[12] below) which is later used in equation (17) to calculate thick-target hard X-rays. In § 2.2 we present a parameterized approximation to the fully collisional current sheet distribution function, which includes the drifting "thermal current" portion.

These results all assume that the electric field is sub-Dreicer ($E \ll E_D$), where the Dreicer field is that (strong) field for which $p_{cr} = p_{th}$, the thermal momentum, and the entire thermal distribution would undergo runaway acceleration, i.e., macroscopic accelerated mass motions would take place. While such high fields may be present at times in the solar atmosphere, they are not allowed for in our analysis. Note that the presence of currents is assumed in this model, but how they arise is immaterial. Specifically, the currents may or may not be associated with magnetic reconnection.

2.1. *The Runaway Distribution*

A competely accurate distribution function for electrons in an external electric field of finite size has not been obtained to date. Typically, the approximation of an infinite, homogeneous plasma is made and a linearized high-velocity form of the Fokker-Planck equation is solved numerically (e.g., Kulsrud et al. 1973; Wiley & Hinton 1980; Fuchs, Cairns, & Lashmore-Davies 1986). Since we will make extensive use of the distribution function in the bremsstrahlung integrand, our goal is to obtain a realistic, yet computationally simple approximation to it. Since runaways exist only at momenta $p > p_{cr}$, the only force present in our analysis is due to the electric field, E. We do allow for particles to be lost from the current sheet, through a parameterized loss term, without specifying the physics of the scattering involved. Thus both classical and anomalous processes are allowed for in this one-dimensional analysis. The neglect of the electrons' gyration is justified if the gyroradius is less than the shortest distance across the current channel. This places a lower limit on the magnetic field strength for which this analysis is valid. We discuss this further in § 3.1.

Details of the runaway process can be found in Holman (1985; with the relativistic velocity $v \rightarrow p/\gamma m$, where p is momentum, γ is the Lorentz factor, and m is the electron mass). Explicitly, we have that

$$\frac{p_{cr}}{mc} = \frac{(p_{th}/mc)}{\sqrt{\epsilon - (p_{th}/mc)^2(1-\epsilon)}}, \tag{1}$$

and

$$\frac{p_{th}}{mc} = \left(\frac{mc^2}{kT} - 1\right)^{-1/2}. \tag{2}$$

The parameter $\epsilon \equiv E/E_D$ measures the electric field strength as a fraction of the Dreicer field. It is constrained by $(kT/mc^2) < \epsilon \ll 1$. The lower limit arises from relativistic effects (Connor & Hastie 1975) while the upper limit ensures that the field is "weak," i.e., it produces a nonthermal tail of runaways without greatly displacing the entire bulk thermal population. The critical energy, $\mathscr{E}_{cr} = [\gamma(p_{cr}) - 1]mc^2$, is that energy at which the systematic acceleration is just balanced by the retardation effects of collisions. At energies below $\mathscr{E}_{cr}$ the electrons are not freely accelerated and serve mainly to heat collisionally the ambient plasma. Thus $\mathscr{E}_{cr}$ serves as the low-energy cutoff to the nonthermal electron population.

We follow a continuity argument within an element of current sheet, dx, allowing runaway losses, $\mathscr{L}$. Thus

$$(p + dp)f(x + dx, p + dp) = pf(x, p) - \mathscr{L}f(x, p)dx . \quad (3)$$

Technically, there should be a source term on the right-hand side of equation (3) representing particles scattered into the current sheet element, per unit time, with momentum p. Since these will overwhelmingly be particles collisionally scattered up from lower momenta ($p < p_{cr}$) within the current sheet itself, we will absorb this term in our boundary condition.

The finite length L of the acceleration region means that a freely accelerated electron beginning with p_{cr} will attain a maximum cutoff energy, $\mathscr{E}_{co} = [\gamma(p_{co}) - 1]mc^2$ with

$$p_{co}/mc = \{[\gamma(p_{cr}) + eEL/mc^2]^2 - 1\}^{1/2} . \quad (4)$$

The boundary condition will be that our solution match, at p_{co}, a numerical solution from the plasma physics literature, of the Fokker-Planck equation for this problem (Fuchs et al. 1986, 1988). This condition is chosen at p_{co} because our collisionless assumption is most nearly matched by the fully collisional numerical solution at the highest attainable momenta. The numerical solution at p_{co}, given below, will be designated $f_{Num}(p_{co})$.

After rearranging and linearizing equation (3), we obtain

$$\frac{df}{dx} + \left(\frac{1}{p}\frac{dp}{dx} + \frac{\mathscr{L}}{p}\right)f = 0 , \quad (5)$$

subject to $f(p_{co}) = f_{Num}(p_{co})$.

The numerical solution is for an infinite, homogeneous plasma, and thus does not allow for losses ($\mathscr{L} = 0$), leading to the constant of integration $C = (p_{co}/p_{cr})f_{Num}(p_{co})$.

We model the particle losses as

$$\mathscr{L} = (p/p_{th})^{\alpha}(p_{th}/l) , \quad (6)$$

where l is the scale length for the losses (mean free path in the current sheet) and α provides the momentum dependence of the losses. The case of no losses ($\mathscr{L} = 0$) is obtained by letting $l \to \infty$ (or $\alpha \to -\infty$).

Using equation (4) and $dx = (mc^2/eE)d\gamma$, we obtain the distribution function for electrons undergoing runaway acceleration in a current sheet of length L:

$$f_{rw}(L, p) = \frac{p_{co}}{p} f_{Num}(p_{co}) \times \exp\left[\frac{-mc^2}{eEl}\left(\frac{p_{th}}{mc}\right)^{1-\alpha}\int_{\gamma_{cr}}^{\gamma}(\gamma'^2 - 1)^{(\alpha-1)/2}\,d\gamma'\right] . \quad (7)$$

Note that the exponential factor is unity for $\mathscr{L} = 0$, in which case $f_{rw} \sim p^{-1} \sim \mathscr{E}^{-1/2}$.

The normalization for equation (7) is given by Fuchs et al. (1986, 1988):

$$f_{Num}(p_{co}) \simeq \frac{\Gamma}{\epsilon}\left\{1 + \frac{2 + \bar{Z}_i}{\epsilon[(p_{co}/p_{th})^2 + 3T_\perp]}\right\} ; \quad (8)$$

$$T_\perp(p_{co}) = \frac{(p_{co}/p_{th})^2}{6}\left[-1 + \sqrt{1 + \frac{12T_\infty}{(p_{co}/p_{th})^2}}\right] ; \quad (9)$$

$$T_\infty = \left(\frac{1 + \bar{Z}_i}{2\epsilon}\right)\ln\left[1 + \epsilon\left(\frac{p_{co}}{p_{th}}\right)^2\right] . \quad (10)$$

Kinetic theory yields the following result for the relativistically accurate runaway production rate, allowing for a background of ions having average charge $\bar{Z}_i$ (= 1.2 for the corona) in units of the proton's charge (Kruskal & Bernstein 1962; Connor & Hastie 1975; Cohen 1976; Singh 1977):

$$\Gamma = (0.3 + 1.5\epsilon)\epsilon^{(-3/16)(\bar{Z}_i+1)} \times \exp\left[\frac{-kT}{mc^2}\left(\frac{1}{8\epsilon^2} + \frac{2}{3\epsilon^{3/2}}\sqrt{\bar{Z}_i + 1}\right) - \left(\sqrt{\frac{\bar{Z}_i + 1}{\epsilon}} + \frac{1}{4\epsilon}\right)\right] \quad (11)$$

The solution, equation (7), is valid in the runaway regime, i.e., for $\mathscr{E}_{cr} < \mathscr{E} < \mathscr{E}_{co}$. In our approximation we must set $f_{rw} = 0$ for $\mathscr{E} < \mathscr{E}_{cr}$, since collisons prevent runaway acceleration from occurring. In fact, the cutoff should not be that sharp. Since $\mathscr{E}_{cr}$ physically describes a balance between collisions and acceleration, we expect that f_{rw} will rise more gradually with energy than our approximation allows, achieving its value of equation (7) at an energy near $\mathscr{E}_{cr}$. The low-energy drifting Maxwellian and a correction for this sharp cutoff below $\mathscr{E}_{cr}$ are obtained in the next subsection.

Particles having $\mathscr{E} > \mathscr{E}_{co}$ are assumed to follow a Maxwellian distribution, since they originate from particles with $p > p_{cr}$ in the original Maxwellian distribution near the origin of the current sheet. They do not necessarily have the same temperature as the plasma from which they were drawn, however. Equation (9) is a measure of the spread in the distribution function, perpendicular to the acceleration direction, in units of the original temperature. At the end of the acceleration region, for $p > p_{co}$, we expect the parallel distribution to be characterized also by the temperature $T_\perp(p_{co})$. Thus, above p_{co}, the expression for f becomes

$$f_{co} = f_{rw} \times \exp\left[\frac{-mc^2}{kTT_\perp(p_{co})}(\gamma - \gamma_{co})\right] , \quad (12)$$

to give the high-energy Maxwellian. The origin of $T_\perp$ is not entirely known, but Kulsrud et al. (1973) suggested it may be due to the Joule heating. This is the least certain aspect of the distribution function. We shall see, however, that this choice for the electron distribution above $\mathscr{E}_{co}$ is consistent with the flare X-ray data. Our fits typically give values of $T_\perp \sim$ a few $\times 10^8$ K. The data cannot be acceptably fitted with a value of $T_\perp$ that is as low as the bulk thermal temperature, or that is much higher than the value used here.

For a perfect accelerator $\mathscr{L} = 0$, leading to $f_{rw} = (p_{co}/p)f_{Num}(p_{co}) \sim \mathscr{E}^{-1/2}$. This is slightly softer than found in the numerical solutions for an infinite, homogeneous plasma. Preliminary results from a detailed study of the Fokker-Planck solution for the case of a *finite* current sheet indicate that the runaway plateau does indeed closely follow a $1/p$ dependence at large values of p (P. MacNeice, private communication). The integral in equation (7) can be performed analytically for α = integer. For nonintegral α, the integral is easily done numerically and is computationally simpler than solving the Fokker-Planck equation.

2.2. *The Collisional Current Sheet Distribution*

For completeness we give here our approximation to the fully collisional current sheet electron distribution function. To zeroth order, the Spitzer-Härm solution (Spitzer & Härm 1953) or its relativistic counterpart, the Hakim-deGroot distribution (Hakim 1967; deGroot, van Leeuwen, & van Weert 1980) can be used. This is given by

$$f_{\mathrm{HdG}}(x, p) = \exp\left\{\mathscr{N} - \gamma_{\mathrm{dr}} \frac{mc^2}{kT}\left[\gamma(p) - \frac{p}{mc}\frac{p_{\mathrm{dr}}}{mc} - \frac{eEx}{mc^2}\right]\right\}. \quad (13)$$

Here $\mathscr{N}$ is a normalization constant, $p_{\mathrm{dr}} = \epsilon p_{\mathrm{th}}$ is the "drift momentum" of the thermal current due to the electric field E, and $\gamma_{\mathrm{dr}} = \gamma(p_{\mathrm{dr}})$. No pitch angle effects are included here in our one-dimensional analysis of the parallel distribution. In general, $\mathscr{N}$ must be determined numerically.

In this approximation, the entire current sheet distribution function is given by

$$f_{\mathrm{cs}} = f_{\mathrm{HdG}} + f_{\mathrm{rw}} ,$$

where f_{rw} is obtained from equation (7). It is known, however, that equation (13) can severely underestimate the number of particles with $p > p_{\mathrm{th}}$, and thus the important regime of $p_{\mathrm{th}} < p < p_{\mathrm{cr}}$ is treated quite poorly in this approximation. This regime has no satisfactory analytic treatment and yet is crucial to the runaway process.

We have parameterized the existing numerical solutions in this region of momentum space. This approach can very simply reproduce the numerically derived distribution function of Fuchs et al. (1988) over their full range of ϵ (from 0.04 to 0.1), to within a factor of 1.5. The complete distribution function of electrons in a current sheet is then given, in four distinct regions of momentum space, by

$$f_{\mathrm{cs}} = \begin{cases} f_{\mathrm{HdG}} + RMf_{\mathrm{rw}} & \text{for } p \le p_{\mathrm{co}} , \\ f_{\mathrm{HdG}} + Mf_{\mathrm{co}} & \text{for } p > p_{\mathrm{co}} , \end{cases} \quad (14)$$

where

$$R = \begin{cases} 0 & \text{for } p < p_{\mathrm{th}} , \\ \sin\left[\left(\frac{\pi}{2}\right)\frac{p - p_{\mathrm{th}}}{p_{\mathrm{cr}} - p_{\mathrm{th}}}\right] & \text{for } p_{\mathrm{th}} \le p \le p_{\mathrm{cr}} , \\ & \text{for } p > p_{\mathrm{cr}} , \end{cases} \quad (15)$$

$$M = 1 + \frac{(p_{\mathrm{cr}}/p_{\mathrm{th}})[(p_{\mathrm{cr}}/p_{\mathrm{th}}) - 2]}{\pi\{1 + [(p/p_{\mathrm{th}}) - 2/3(p_{\mathrm{cr}}/p_{\mathrm{th}})]^2\}} , \quad (16)$$

and f_{HdG}, f_{rw}, and f_{co} are given by equations (13), (7), and (12), respectively.

3. THERMAL/NONTHERMAL HARD X-RAYS

The presence of coronal currents in a flaring region on the Sun provides for both accelerating particles (the runaway process) and heating the ambient plasma (Joule dissipation). We can thus expect simultaneous contributions of both nonthermal and thermal bremsstrahlung to the observed hard X-rays. The thermal emission reflects the temperature of the current sheets, which is presumably the highest temperature plasma in the flare, i.e., the superhot component. This component will be distinctly observable when enough of the surrounding plasma has been heated, that is, when its emission measure becomes large enough. The nonthermal emission is assumed to be thick target.

There are five free parameters in this model: the temperature T and emission measure EM of the thermal plasma; the low-($\mathscr{E}_{\mathrm{cr}}$) and high-($\mathscr{E}_{\mathrm{co}}$) energy cutoffs for the runaway electrons; and the area A of the thick-target emission. In order to obtain an electric field strength, a length L of the current sheet must be assumed or deduced from high spatial resolution imaging. If particle losses from the current sheet are required, two more parameters (α and l) are needed. In the standard modeling with a broken power-law fit to nonthermal hard X-rays and using T and EM for the superhot thermal hard X-rays, six independent parameters are required. The number of free parameters is reduced by one in this model because the parameters are physically coupled.

Before proceeding further, it is desirable to discuss some possible spatial relationships between current sheets and the thick-target chromosphere. If a coronal current sheet is anchored in the chromosphere (e.g., aligned along an entire magnetic loop), it is possible that the entire current sheet population, i.e., equation (14), will produce thick-target emission. This allows the counterintuitive possibility that the low-energy hard X-rays, while appearing thermal, are actually due to thick-target bremsstrahlung from the "thermal current" electrons in the current sheet. The current will still heat the ambient coronal plasma, generating true thermal emission. The relative importance of the two processes at low hard X-ray energies cannot be determined from the spectra. Arcsecond spectrally resolved hard X-ray imaging of a flare at the limb could help.

For this same geometry, a second possibility is that there exists a temperature gradient along the current sheet. In this case, even if the currents are anchored in the cooler chromosphere, only the runaways would contribute significantly to the hard X-ray emission. The "thermal current" would not be energetic enough at the location of the thick target.

A third possibility is that the current sheet does not lead directly to the chromosphere, but lies wholly in the corona. In this case, the thick-target emitting electrons must first escape the current sheet, then stream down magnetic field lines (such as in an arcade) to impact the chromosphere. It is likely that the lower energy electrons will remain in the current sheet, and again only the runaways will produce thick-target emission.

In this paper we will assume that the thick-target emission is from runaway electrons only, while the thermal component is from heated plasma in the corona.

The loss term, $\mathscr{L}$, has a dual role in all of this. It is clear from its introduction in equation (3) that it represents particle loss from the acceleration region. However, once it is convolved in the bremsstrahlung integrand (eq. [17] below) it also represents the loss of particles from the thick-target hard X-ray–producing population. In the first two cases discussed above, these roles coincide. When an electron is lost from the current channel it is also lost to the thick target. The third case is not as clear. Since the thick-target emitting electrons have already escaped from their current channels, does the loss term describe this escape or a further loss of particles in transit to the thick target? It is at this point that we must recognize that there are no geometrical constraints inherent in this model, i.e., a unique cartoon cannot be drawn. Indeed, recent observations (Willson, Lang, & Gary 1993) show that particle acceleration in flares may take place in geometries very different from the usual cartoons. For this reason we prefer to let the spatial aspects of this model be guided by (future) high-resolution imaging, particularly in hard X-rays. In the meantime, since the radiation is the observable, we must accordingly approach $\mathscr{L}$ as characterizing losses from the radiating population, without knowing if those losses occurred in the current sheet or in transit to the emission region.

An electron of kinetic energy $\mathscr{E}$ can generate bremsstrahlung photons of all energies $\epsilon \leq \mathscr{E}$, but care must be taken in this model in deciding what electron energies to consider. The differential thick-target bremsstrahlung hard X-ray flux is given by (Brown 1971, with the correct factor of π, cf. Lin & Hudson 1976):

$$I_{\rm tt}(\epsilon) = 1.345 \times 10^{-24} \frac{N_r A}{\epsilon p_{\rm th} \ln \Lambda} \int_{\mathscr{E}_{\rm min}}^{\mathscr{E}_{\rm max}} f(\mathscr{E}; \alpha, l)\left(1 + \frac{\mathscr{E}}{mc^2}\right) \times \int_{\epsilon}^{\mathscr{E}} \bar{Z}_i^2 \ln \left\{\frac{1 + \sqrt{(1 - \epsilon/\mathscr{E}')[1 - \epsilon/(\mathscr{E}' + 2mc^2)]}}{1 - \sqrt{(1 - \epsilon/\mathscr{E}')[1 - \epsilon/(\mathscr{E}' + 2mc^2)]}}\right\} d\mathscr{E}'\, d\mathscr{E} , \tag{17}$$

where $f(\mathscr{E}; \alpha, l)$ is the electron energy distribution function for the radiating electrons (density N_r) which reach the thick-target (effective surface area A). [We have replaced the electron flux density, $F(v)$, with $F(v) = f(v)p/m$.] We use coronal elemental abundances (Meyer 1985), so the average charge state of the fully ionized flare plasma is $\bar{Z}_i = 1.2$. Although more accurate bremsstrahlung cross sections are now available (Johns & Lin 1992), the form used here is valid for ϵ up to $\sim$400 keV. The lower limit of integration, $\mathscr{E}_{\rm min}$, is the greater of either ϵ or $\mathscr{E}_{\rm cr}$ if only runaway electrons produce thick-target emission (using eqs. [7] and [12]) as in the next subsection. If the entire current sheet distribution (runaways + thermal current, eq. [14]) is used, the lower limit is always ϵ, the photon energy.

The runaway electron distribution generates an X-ray spectrum which is apparently softer than the electrons, due to significant contributions of high-energy electrons to the low-energy emission. A 100 keV electron produces 50 times more 20 keV photons than does a 25 keV electron, and 7 times more than does a 40 keV electron. For runaways ($f \sim \mathscr{E}^{-1/2}$), the number of 25 keV and 100 keV electrons differ by only a factor of 2, and it is clear that the overwhelming contribution to low-energy photons will arise from the large number of high-energy electrons. This enhanced low-energy emission makes the spectrum appear softer than the electrons (the photon spectral index is about 1.5 when the electron spectral index is 0.5), regardless of the collisional degradation of the low-energy electrons. For comparison, an electron distribution $f \sim \mathscr{E}^{-5}$ has 1000 times more 25 keV than 100 keV electrons, and so the collisional losses of the low-energy electrons in the thick target degrade the low-energy part of the X-ray spectrum, making it harder.

The differential thermal bremsstrahlung X-ray flux is (Tucker 1975; Crannell et al. 1978):

$$I_{\rm th}(\epsilon) = 1.07 \times 10^{-42} \frac{\sum_i {\rm EM}_i Z_i^2}{\epsilon\sqrt{kT}} \bar{g}_{\rm ff}\, e^{-\epsilon/kT} = \frac{1.3 \times 10^{-42}\,{\rm EM}}{\epsilon^{1.4}(kT)^{0.1}} \times \exp\left(-\frac{\epsilon}{kT}\right) \text{ photons cm}^{-2}\,\text{s}^{-1}\,\text{keV}^{-1} , \tag{18}$$

using $\sum_i {\rm EM}_i Z_i^2 = 1.2$ EM, with the emission measure EM $= N_e^2 V$. The Gaunt factor is approximated by $\bar{g}_{\rm ff} = (kT/\epsilon)^{0.4}$.

3.1. *The 1980 June 27 Flare*

We have used the above formalism to model in detail the flare of 1980 June 27 (Lin et al. 1981) observed with a high spectral resolution germanium detector. We assume that runaway electrons produce thick-target bremsstrahlung (using eqs. [7]–[12] in eq. [17]) while thermal bremsstrahlung (eq. [18]) is generated simultaneously in plasma heated to the temperature of the current sheets. Thus we fix T, $\mathscr{E}_{\rm cr}$, and $\mathscr{E}_{\rm co}$ (also α and l if $\mathscr{L} \neq 0$), calculate both thermal and nonthermal X-rays at each photon energy in the given spectrum, and adjust EM and A to minimize χ_ν^2 for that set of parameter values. We explore a wide range of parameter space to ensure that the final χ_ν^2 is a global minimum. We assume the length L of the acceleration region to be 3×10^9 cm. The effect of choosing a different value of L will be discussed later.

Lin & Schwartz (1987) and Johns & Lin (1992) have suggested that the hard X-ray emission from this event consists of two physically distinct components, a series of spikes superposed on a more gradually rising and falling component. We confine our analysis to these two components, since our model is physical and not merely descriptive of the data. We obtained 36 spectra, each of 5 s duration, from 1614:44.37 to 1617:44.37 UT. Of these, we found eight which are good examples of the gradual component, i.e., most or all of the 5 s interval is an interspike minimum of the emission. Our fits to these spectra are shown in Figure 1. The individual spectra, here and in Figure 2, are labeled with the time in seconds after 1614:41.87 UT. The fitting parameters are displayed in Figures 3–5 below. In Figure 1 thermal bremsstrahlung is a dashed line and thick-target emission is a dotted line. The deviation of our computed sum of these (*solid line*) at the lowest energies reflects our inclusion of the *GOES* soft X-ray emission as well. The *GOES* temperature and emission measure is given in Tables 1 and 2, and the emission due to this plasma is shown for the spectrum at $t = 175$ as a dot-dash line in Figure 1. It can be seen that this is generally negligible above 15 keV. The spectrum at $t = 60$ actually includes a small spike ($\sim$18% above the gradual component in the 22–33 keV range) which may contaminate this spectrum slightly. We find significant thermal emission for all of these gradual component spectra. The nonthermal emission is fully consistent with that from pure runaway accelerated electrons, i.e., the loss term (and its additional two parameters) was found to be unnecessary for acceptable fits. The reduced χ^2 statistic is given in the tables.

We also examine the three main spikes and a smaller spike at the start of the flare ($t = 10$). Two 5 s spectra were available for each of the three main spikes. We fitted each of these spectra separately, as well as the combined 10 s spectra. The latter are shown in Figure 2 ($t = 87.5$, 107.5, 142.5) along with the earlier spike. In all cases, we interpolated the gradual component emission to the center of the 5 or 10 s spike interval and subtracted this gradual emission, leaving the emission due to the pure spike. This is essential since the spike emission is only about twice the underlying gradual component emission. If the spike were an order of magnitude higher, the subtraction might be unnecessary. It is interesting that the first spike ($t = 10$) is part of a separate gradual component from the main impulsive phase. Most significantly, there is no thermal emission apparent in any of these pure spike spectra. (The fit at $t = 10$ is

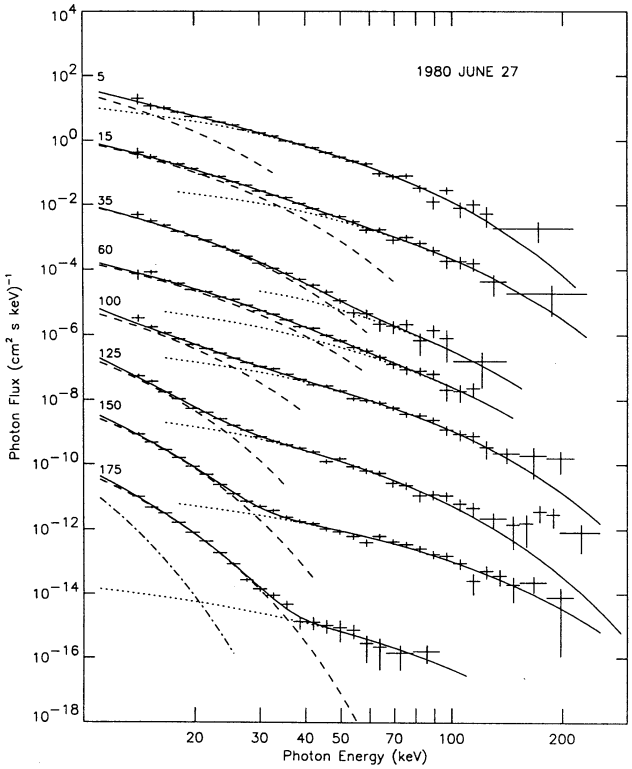

FIG. 1.—Spectra from the gradual component of the 1980 June 27 event, labeled with the time in s after 1614:41.87 UT. The flux of each spectrum after the first is offset by 10^{-2}. The dashed lines show thermal bremsstrahlung and the dotted lines thick-target bremsstahlung from runaway electrons. These lines are truncated to avoid interfering with subsequent spectra. The deviation at the lowest energy is due to the inclusion of thermal *GOES* soft X-ray emission, shown explicitly at $t = 175$ as a dot-dash line. The χ_ν^2-statistic is given in Table 1.

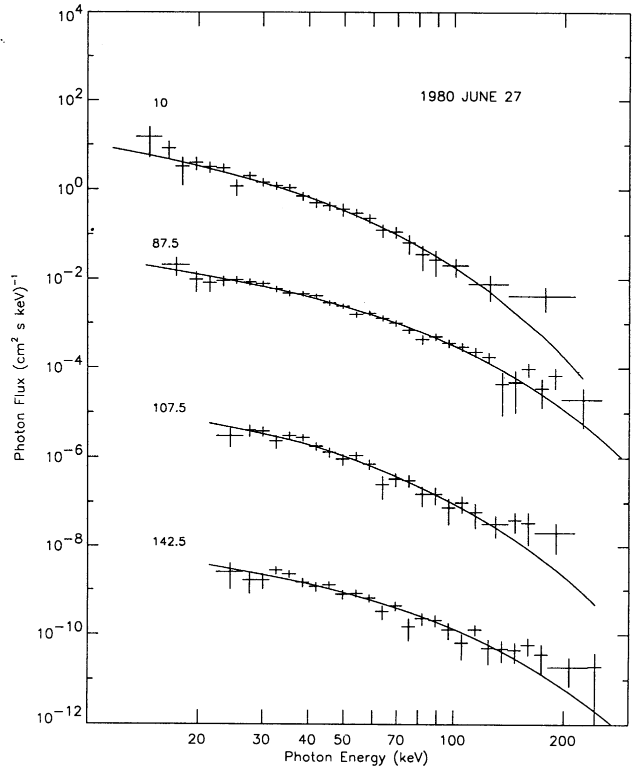

FIG. 2.—Pure spike spectra from the event of 1980 June 27, labeled as in Fig. 1, and offset by 10^{-3}. These data are well fitted with only thick-target emission from runaway electrons. The χ_ν^2-statistic is given in Table 2.

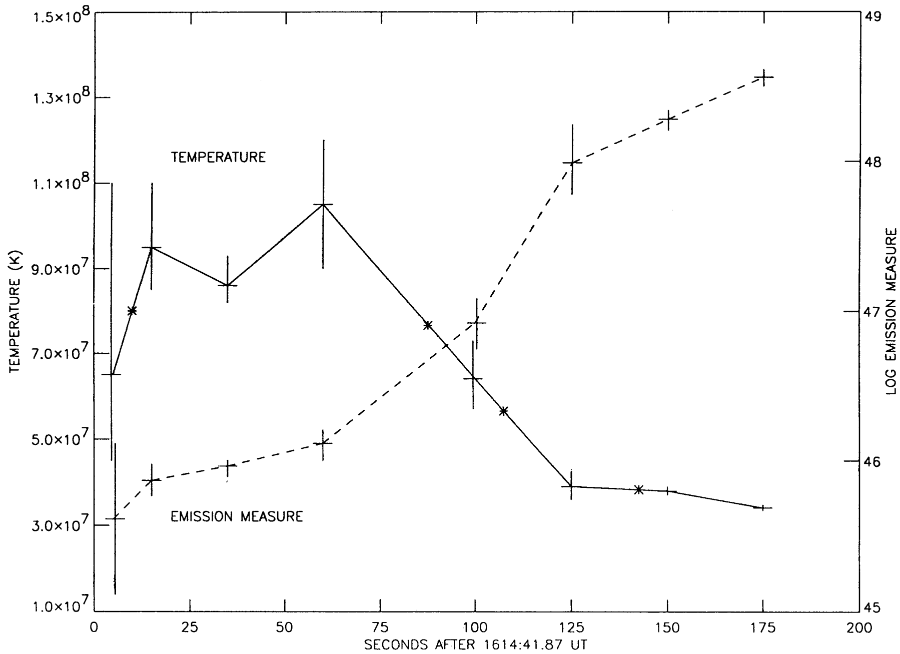

FIG. 3.—The evolution of the temperature (*solid line*) and log (emission measure) (*dashed line*), as derived from the spectral fits of Fig. 1. The asterisks denote the assumed temperature for the spike emission, as discussed in the text.

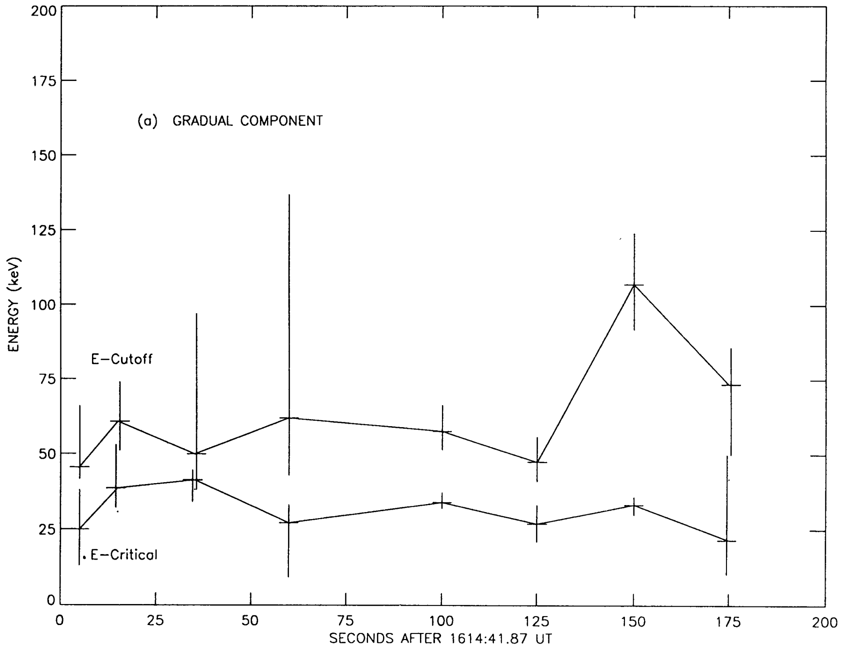

FIG. 4a

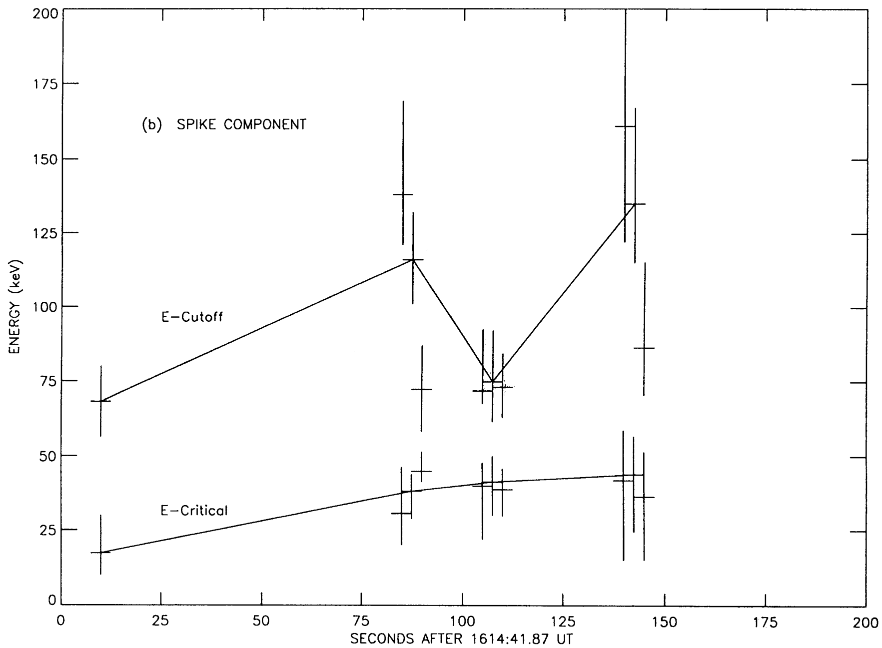

FIG. 4b

FIG. 4.—The evolution of $\mathscr{E}_{cr}$ and $\mathscr{E}_{co}$ for (*a*) the gradual component spectra of Fig. 1 and (*b*) the spike spectra of Fig. 2. In all cases $\mathscr{E}_{co}$ lies above $\mathscr{E}_{cr}$. Some data points in (*a*) have been artificially offset in time by ± 0.5 s to avoid overlapping error bars. In (*b*), the solid lines connect the results for 10 s intervals at t = 87.5, 107.5, and 142.5. The results on either side of these points are for the two 5 s intervals of which the longer interval was composed.

improved slightly by including thermal emission. The displayed fit—$\chi_\nu^2 = 0.63$—is already so good, however, that the extra two parameters cannot be justified.) Once again, the observed nonthermal emission is consistent with pure runaway acceleration, i.e., the $\mathscr{E}^{-1/2}$ runaway plateau (from $\mathscr{E}_{cr}$ to $\mathscr{E}_{co}$) in the electron distribution extends over a broad energy range for the four spectra. The third free parameter for these fits is the normalization. Without any temperature information, the area cannot be separated out of this normalization. By making the assumption that the temperature in these spikes is the same as that of the gradual component at the same time (the asterisks in Fig. 3), we obtain the areas shown as asterisks in Figure 5. Both the count statistics and the fact that the emission at the lowest energies rises continually through the event (below ~25 keV it is not spikey) preclude our getting reliable data from the subtraction process at photon energies lower than shown.

Figures 3–5 show the evolution of our fitting parameters for this event. The error bars were determined by mapping out the

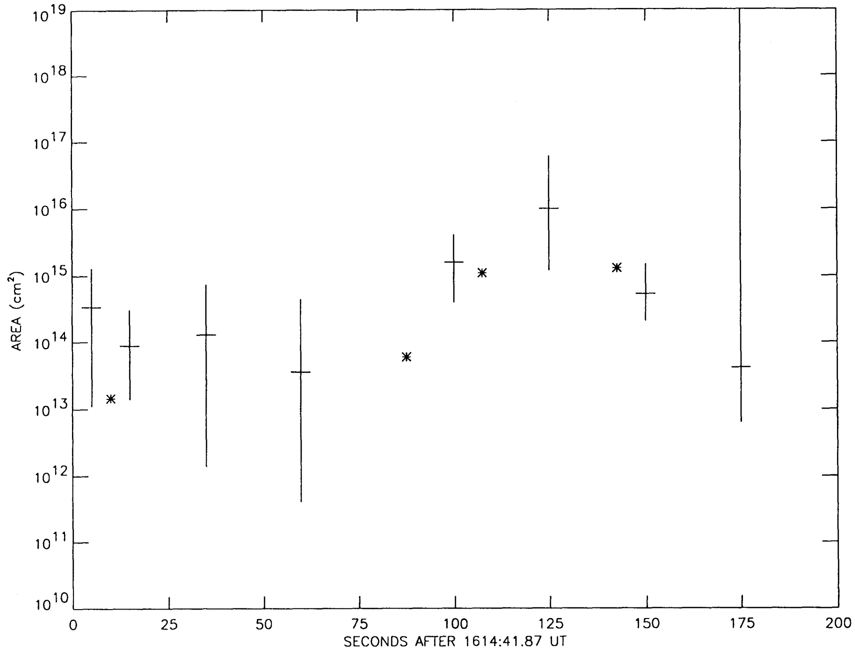

FIG. 5.—The evolution of the thick-target area derived from the spectral fits of Fig. 1. The asterisks denote the areas that would result from assuming the temperatures shown in Fig. 3 for the spikes.

contours in parameter space for which χ_ν^2 is increased by 5% from its minimum value, and finding the extrema of each parameter's contours in this three- or five-dimensional domain. There exist many local χ_ν^2 minima in this domain, each having its own contours. Nevertheless the maximum extent of the entire collection of contours necessarily encompasses the global minimum, and it is this extent which is reflected in our vertical error bars. For each time interval, the indicated parameter values produced the lowest χ_ν^2 that we could find, in turn defining the 5% contour level. It is conceivable that some other combination will produce a slightly smaller χ_ν^2, but since this would in turn shrink the error bars, it is certain that the true global minimum falls within the range depicted. Some data points in Figures 3 and 4 have been offset by ± 0.5 s in

TABLE 1

DERIVED PARAMETERS FOR 1980 JUNE 27 FLARE: GRADUAL COMPONENT

	GRADUAL COMPONENT								
	Time (s) after 1614:41.87 UT								
PARAMETER	5	15	35	60	100	125	150	175	UNITS
ϵ	0.121	0.119	0.101	0.180	0.089	0.067	0.054	0.072	E/E_D
E	23	25	9.7	39	26	23	82	58	10^{-9} sv cm^{-1}
ν_{th}	32	29	14	28	50	73	330	180	s^{-1}
n^J	6.0	9.6	3.9	11	9.3	6.6	30	14	10^{10} cm^{-3}
η^{cl}	2.1	1.2	1.4	1.0	2.1	4.4	4.4	5.2	10^{-18} s
dN/dt	140	57	13	110	340	340	43	8.2	10^{32} s^{-1}
$d\mathscr{E}/dt$	110	64	14	110	350	290	62	8.0	10^{25} ergs s^{-1}
Q	120	90	31	78	800	1400	630	19	10^{25} ergs s^{-1}
V^Q_{min}	1.1	0.80	5.9	1.1	9.5	220	20	180	10^{24} cm^3
V^J	4.8	1.7	4.6	0.51	25	120	4.1	0.29	10^{24} cm^3
n^Q_{max}	2.9	6.6	3.9	11	5.8	6.6	30	14	10^{10} cm^{-3}
t^J	0.50	1.1	8.8	2.3	1.0	5.4	5.0	630	s
	$B = 120$ G and $w = L/3 = 10^9$ cm								
δr	52	27	83	15	46	110	31	51	cm
dN/dt/sheet	45	27	7.1	95	19	9.7	9.8	43	10^{28} s^{-1}
s	31	21	18	12	180	350	44	1.9	10^3
A^J/A	4.8	6.6	11	4.7	5.0	3.7	2.6	2.3	
	Supplementary Information								
GOES T	1.1	1.2	1.2	1.2	1.5	1.6	1.6	1.7	10^7 K
GOES EM	1.8	2.2	4.1	8.8	19	29	38	46	cm^{-3}
χ_ν^2	0.99	0.71	0.75	0.75	0.74	1.47	0.88	1.10	

TABLE 2

Derived Paramenters for 1980 June 27 Flare: Spike Component

Parameter	Spike Component: Time (s) after 1614:41.87 UT				Units
	10	87.5	107.5	142.5	
ϵ	0.209	0.097	0.066	0.043	E/E_D
E	56	86	37	100	10^{-9} sv cm^{-1}
ν_{th}	41	140	100	520	s^{-1}
n^J	11	35	16	48	10^{10} cm^{-3}
η^{cl}	1.5	1.6	2.5	4.3	10^{-18} s
dN/dt	95	140	96	24	10^{32} s^{-1}
$d\mathscr{E}/dt$	83	210	120	44	10^{25} ergs s^{-1}
Q	38	320	790	2400	10^{25} ergs s^{-1}
V^J	0.18	0.69	14	10	10^{24} cm^3
t^J	0.55	0.79	2.2	1.1	s
$B = 120$ G and $w = L/3 = 10^9$ cm					
δr	15	10	39	25	cm
dN/dt/sheet	240	64	7.8	1.8	10^{28} s^{-1}
s	4.0	67	120	130	10^3
A^J/A	3.3	11	4.4	2.6	
Supplementary Information					
GOES T	1.1	1.5	1.5	1.6	10^7 K
GOES EM	2.0	15	21	36	cm^{-3}
χ_ν^2	0.63	0.92	0.99	1.20	

time, to avoid overlapping error bars. We also point out that, in general, randomly chosen parameter combinations from within the error bars produce unacceptably poor fits. This is because the parameters cannot be arbitrarily decoupled from each other in this physical model.

Fits to the gradual component subtracted from the spikes should provide best-fit parameters that are consistent with those obtained from the gradual component on either side of the spikes. We have checked this, and find that the parameters fall on the curves in Figures 3–5 as expected.

Figure 3 shows a systematic evolution of the temperature, and a monotonic increase of the emission measure for this Joule-heated "superhot" component. The earliest temperature is poorly determined, but it is possible that the initial rapid heating which must accompany flare onset is being seen. In any event, a cooling trend is apparent from before the first main spike until the end of the event. Although the plasma is cooling, the emission measure increases by more than 2 orders of magnitude, reflecting the continual plasma heating by the current sheets, and transport of the heat to an increasing volume. After $t = 125$ the temperature seems to level off, although a slow cooling continues. At the same time the increase in the emission measure begins to taper off. The continuation of both of these trends can be seen in Figure 5 of Lin et al. (1981), and the emission measure of this superhot thermal component actually begins decreasing after $t = 175$. Around $t = 125$ it therefore appears that the flare plasma has achieved some steady-state heat transport in which the heat input from the current sheets into the surrounding plasma is balanced by losses. We quantify this statement later in this section.

Figure 4*a* shows both $\mathscr{E}_{cr}$ and $\mathscr{E}_{co}$ for the gradual component, and Figure 4*b* shows them for the spikes. For each of the three main spikes we show the best-fit $\mathscr{E}_{cr}$ and $\mathscr{E}_{co}$ for the two 5 s intervals, as well as for the 10 s interval. These latter values are connected with the solid line. At each time, the vertical distance between the two parameters gives the extent (in keV) of the electron runaway plateau [or alternatively the total potential drop (in kV) for the currents]. It can be seen that this separation is greater, on average, for the spikes in Figure 4*b* indicating stronger electric fields in the spikes. The potential drop exceeds 100 kV in the earlier portions of the first and third main spikes, while it is less than 50 kV later in these spikes. In contrast, the second main spike shows no evolution in $\mathscr{E}_{cr}$ or $\mathscr{E}_{co}$. The electric field strength actually seems to increase late in the impulsive phase, particularly for the gradual component (Fig. 4*a*), but the more relevant parameter may be the ratio $\epsilon = E/E_D$ which decreases. We return to this point later.

Finally, Figure 5 shows the deduced thick target area. For given temperature, $\mathscr{E}_{cr}$, and $\mathscr{E}_{co}$, the area is well determined. However, slight changes in any of these other parameters can produce large changes in the resulting area, leading to the large error bars. It is nevertheless clear that the area is small, less than 1″ square. This may imply a small filling factor of the current "footprints" within the areas imaged by hard X-ray telescopes.

Tables 1 and 2 show quantities which we can obtain from the primary fitting parameters. For the spike component values (Table 2), all quantities except the electric field strength (E) require the starred temperatures and/or areas of Figures 3 and 5. The time runs horizontally and is given in seconds after 1614:41.87. The first parameter is the ratio of the electric field to the Dreicer field, which depends only on T and $\mathscr{E}_{cr}$ (eq. [1]). The next four parameters, the actual electric field, the thermal collision frequency, electron density, and classical resistivity follow from equation (4) and the definition of the Dreicer field as follows:

$$\mathscr{E}_{co} - \mathscr{E}_{cr} = eEL = e\epsilon E_D L = e\epsilon\left(\frac{m}{e}\frac{p_{th}}{m\gamma_{th}}\nu_{th}\right)L\,, \qquad (19)$$

where p_{th} (and thus γ_{th}) is given in equation (2) and the assumption of constant L is used. The density and resistivity require only the temperature and ν_{th}. Note that all of these parameter values are determined *within the current sheets.* A clear evolution of ϵ is apparent. Table 1 shows that ϵ is always higher before $t = 60$ than after, while Table 2 shows a monotonic decrease in ϵ. The accompanying values of the electric field do not show this pattern, suggesting that the relation of this field to the plasma in which it is embedded (E_D depends on both temperature and density) is more fundamental to the flare phenomenon than the actual value of the field itself. The decreasing value of ϵ is driven by the overall cooling trend as well as a possible (though erratic) increase in density within the current channels.

Having deduced the electron runaway distribution, it is straightforward to integrate it and obtain the nonthermal energetics for this flare. The next two rows give the accelerated electron flux and the energy flux in these electrons. Holman et al. (1989, their eqs. [1] & [2]), showed that the ratio of accelerated electron flux to Joule heating rate (Q) depends only on temperature and ϵ, thus Q follows from dN/dt. Note that Q exceeds $d\mathscr{E}/dt$ as expected, except for the highest values of ϵ, when acceleration may dominate heating (Tsuneta 1985). Next we give a lower limit on the volume of the heated plasma. This uses the emission measure (hence no values for the spike component) and assumes that the average density in the heated plasma, n^Q, is the same as that in the current channels, n^J. Somov (1992, his § 3.2) has shown that in a reconnection region (which is neither required nor excluded by our model) the density outside of the sheets may be lower by a factor of 5 or 6, which would increase V^Q.

We have derived a value for the classical resistivity in the current sheets without having to assume that it applies. The assumption of classical resistivity is probably a good one for this event, however, since (i) we know from the spectral fits (Figs. 1 and 2) that additional scattering and hence turbulence in the current sheets is not necessary, and (ii) our derived values of ϵ are consistent with a classical plasma (Holman 1985; Tsuneta 1985).

If we now make this assumption, we obtain the next three rows of Table 1 and the next two in Table 2. Since $E = \eta J$, and the quantity $\boldsymbol{J} \cdot \boldsymbol{E}$ gives the heating rate per unit volume of the current channels, the total volume of the current channels is $V^J = Q/(\boldsymbol{J} \cdot \boldsymbol{E})$. It is seen in Table 1 that $V^J < V^Q$ as expected except at $t = 5$, 15, and 100, when our assumption of equal densities must be wrong. This sets an upper limit on the density in the heated plasma at these times. At other times, the upper limit is n^J. We also define a heating timescale as

$$t^J = \frac{n^Q kT}{\boldsymbol{J} \cdot \boldsymbol{E}} \frac{V^Q}{V^J} \frac{n^Q}{n^J} . \qquad (20)$$

This is the ratio of the thermal energy in the heated plasma to the Joule heating rate, allowing for different densities and volumes for the heated plasma (n^Q, V^Q) and the current channels (n^J, V^J). To obtain t^J for the spikes, we assume $V^Q/V^J = n^Q/n^J = 1$.

We now return to the notion of steady-state heat transport after $t = 125$, reflected in the values of t^J in the gradual component. At $t = 35$, and again after $t = 125$, the heating timescale is longest, and is at least comparable to the accumulation time of the spectra. At $t = 175$ we see that t^J is very long, but still much shorter than the radiative cooling time for these densities and temperatures. At all of these times, the temperature (Fig. 3) is seen to level off and the emission measure increases more slowly than at other times. In contrast, when the temperature and emission measure change the fastest, t^J is smallest. It is thus possible that a short Joule heating timescale is associated with the onset of the impulsive phase, while the subsequent increase in t^J signals the end of this phase. The value of t^J in the spikes is quite small, suggesting that the reason we do not see thermal emission in the spikes is that the plasma may be unable to remove the excess heat fast enough. An increasing temperature in the current channels decreases the Dreicer field, and thus the electric field (for constant ϵ) during the spike, which could ultimately regulate the duration of the spike itself. The decreasing electric field can be seen in Figure 4*b* in the rapidly decreasing values of $\mathscr{E}_{\rm co}$ in two of the three main spikes. Speculating one step further, the long t^J at $t = 35$ may be signaling the end of the initial gradual component.

It is important to check whether runaway acceleration will take full effect within the 5 s allowed by our spectra. The time required for an electron to be accelerated from $\mathscr{E}_{\rm cr}$ to $\mathscr{E}_{\rm co}$ is $t_{\rm acc} = (p_{\rm co} - p_{\rm cr})/eE$ and all time intervals that we examined have $t_{\rm acc}$ between 0.19 and 0.29 s. The time needed to form a tail of runaways is on the order of a collision time for an electron with $p = p_{\rm cr}$, i.e., $\tau_T = (p_{\rm cr}/p_{\rm th})^3/\nu_{\rm th}$. This is always $\lesssim 1$ s except at $t = 35$ where $\tau_T = 2.7$ s. There is ample time in 5 s for a runaway tail to form and for the electrons to be accelerated.

If we assume a reasonable value for the average induction magnetic field strength $B = 120$ G, and for the width of the current sheets, $w = L/3 = 10^9$ cm, we can derive the next four quantities shown in Tables 1 and 2. This width is consistent with a sheet on the surface of a loop with an aspect ratio of 20, although there is nothing in the model which demands such a location for the current. This magnetic field strength is the weakest that this specific geometry would allow, as we now show. Assuming a laminar current, the sheet thickness, $\delta r = (c/2\pi)(B/J)$, is constrained by Ampere's law (Holman 1985). The current sheets are quite thin. A 100 keV electron moving perpendicular to a 120 G magnetic field has a gyroradius of 6.3 cm which is only slightly less than the deduced sheet thickness for the spike at $t = 87.5$. The gyroradius scales inversely with B so stronger magnetic fields will be stable to the runaway process, justifying our neglect of spiraling motions. The number of runaway accelerated electrons per sheet is found from equation (2) of Holman et al. (1989), but using the better value for Γ, equation (11). Comparing that with dN/dt in the tables, we can deduce the number, s, of current sheets required to satisfy the energetics for this event. They must occur in oppositely directed pairs to limit the total induction magnetic field. We discuss this topic further in the next section. As a consistency check, the values of $V^J = sLw\delta r$ are the same as deduced earlier. Finally, $A^J = sw\delta r$ is the total cross sectional area of the currents, which is consistently larger than the deduced thick-target area, A. This may mean that the currents are not anchored to the thick target. One possibility is that they are confined within that proton of a magnetic loop or arcade which has expanded in the low-β corona. This coronal confinement may be due to temperature or density gradients, as mentioned at the beginning of this section. We also point out that the generally accepted strong unidirectional currents inferred from vector magnetogram data are now being called into question (Wilkinson, Emslie, & Gary 1992) so that the currents which we are discussing are not necessarily related to the vector magnetograms.

We could also assume filled cylinder, filamentary, threadlike geometry (Holman 1985) for the current channels. The value of δr then becomes the radius of the thread, and this greatly increases the number of channels required. For example at $t = 100$, dN/dt/thread $\sim 2.6 \times 10^{22}$ s^{-1} requiring $s = 1.3 \times 10^{12}$. This implies that the individual current channels run along individual (or at most very small bundles of) magnetic field lines.

The maximum allowable runaway flux per sheet is given by (Holman 1985)

$$\dot{N}_{\rm max} = \frac{c}{2\pi e} wB \approx 1.2 \times 10^{30} \ {\rm s}^{-1} , \qquad (21)$$

and this is violated in the earliest spike. This probably indicates that our assumed $T = 8.0 \times 10^7$ K for this spike is too high. Using $T = 3.2 \times 10^7$ K, the accelerated electron flux per sheet is 1.1×10^{30} s^{-1}, so that temperatures up to this value are acceptable. This also decreases ϵ to 0.088 and increases the heat flux to $Q = 5.6 \times 10^{26}$ ergs s^{-1} which now exceeds the nonthermal energy flux, $d\mathscr{E}/dt = 5.0 \times 10^{26}$ ergs s^{-1}. Since the electron flux required for this spike is now reduced to $\sim 5.8 \times 10^{33}$ s^{-1}, the required number of current sheets is changed to $s \sim 5300$. As mentioned earlier, the theoretical fit to this spike was improved slightly by including thermal emission, although statistically this inclusion could not be justified. It is suggestive that the best fit that we obtained was for

$T = 2.5 \times 10^7$ K, and the above analysis indicates that $T \leq 3.2 \times 10^7$ K is required. It is possible that the current sheet temperatures of the spikes are much cooler than the gradual component temperatures which we assumed. $\mathscr{E}_{cr}$, $\mathscr{E}_{co}$, and the electric field strength E are unaffected by a change in temperature, but if the temperature still varies in the same manner as we assumed, the overall evolutionary trends of the spike parameters will still hold, though their actual values will change.

We now address our choice of current sheet length, $L = 3 \times 10^9$ cm. This value is consistent with the reported Hα flare, which had an apparent area of $\sim 1.5 \times 10^{18}$ cm^2 and was quite far from disk center (S25 W67). However, the choice is completely arbitrary for fitting the spectra. Any other value yields the same T, EM, $\mathscr{E}_{cr}$, $\mathscr{E}_{co}$, and χ_ν^2. The resistivity, and all of the ratios ϵ, V^Q/V^J, and A^J/A are also unchanged. The flare energetics change somewhat as shown in the preceding paragraph. We looked at the possibility of a much shorter $L = 3 \times 10^8$ cm (and $w = L/3$). The electric field strength increases by an order of magnitude, as does the density, collision frequency, and number of current sheets. The quantities that are reduced by a factor of 10 are the thick-target area, current sheet thickness, and $\dot{N}$/sheet. The volumes are 100 times smaller. This value of w is unacceptably small, at least at $t = 87.5$, because $\delta r = 1$ cm is less than the gryroradius of a 100 keV electron moving perpendicular to a $B = 120$ G magnetic field. The densities also get uncomfortably high.

Finally, having deduced the runaway electron distribution which generates the spike emission, we can directly compare it with that of Johns & Lin (1992), who inverted the photon spectrum for the first main spike ($t = 85$) to obtain the electron distribution which produced it. We show this comparison in Figure 6, where the data are from Johns & Lin and our deduced electron distribution is the dashed line. It can be seen that the agreement, especially above $\mathscr{E}_{co}$, is excellent. The shape of our distribution was discussed following equation (11). We discuss this figure further in the next section. Lin & Johns (1993) show another inversion of this spike with a 20 s time integration. Our 10 s integration results are consistent with this inversion as well.

4. DISCUSSION

We believe that the extremely hard X-ray spectra for the pure spike component seen in Figure 2 (first noted by Lin & Schwartz 1987) is a signature of DC electric field acceleration. The ubiquity of these very hard spectra—in different spikes, in different time intervals of the same spike, and over different time integration periods for the same spike—is an indication that runaway electron acceleration is occurring. The runaway electron distribution has an unavoidably hard spectral index of $\frac{1}{2}$, and this is reflected in the resulting hard X-ray spectra, over energy ranges from 30 to 100 keV, as we have shown. In order to obtain this signature, however, one needs both high time resolution and high counting statistics to separate adequately the gradual and spike components. In our initial modeling of the 1980 June 27 event (Holman & Benka 1992), we selected two spectra having lower time resolution from those published in Lin et al. (1981). We fortuitously obtained good fits to them with the same simple model ($\mathscr{L} = 0$) that we used in the last section. We subsequently fitted the first 10 spectra from Lin et al. (1981), only four of which were adequately fitted this way. The remaining spectra had best-fit χ_ν^2 ranging from 1.8 to 2.2. To get acceptable fits, we were forced to include the additional parameters α and l. Lacking higher time-resolution data, we would have erroneously concluded that particle losses were required ($\mathscr{L} \neq 0$), engendered by some form of wave turbulence. Thus the lower time resolution data, necessarily blending both gradual and spike components, would lead to the opposite conclusion from that obtained in the previous section, namely that scattering within the current sheets would be needed to explain this event. A similar wrong conclusion is reached if the gradual component is not removed from the

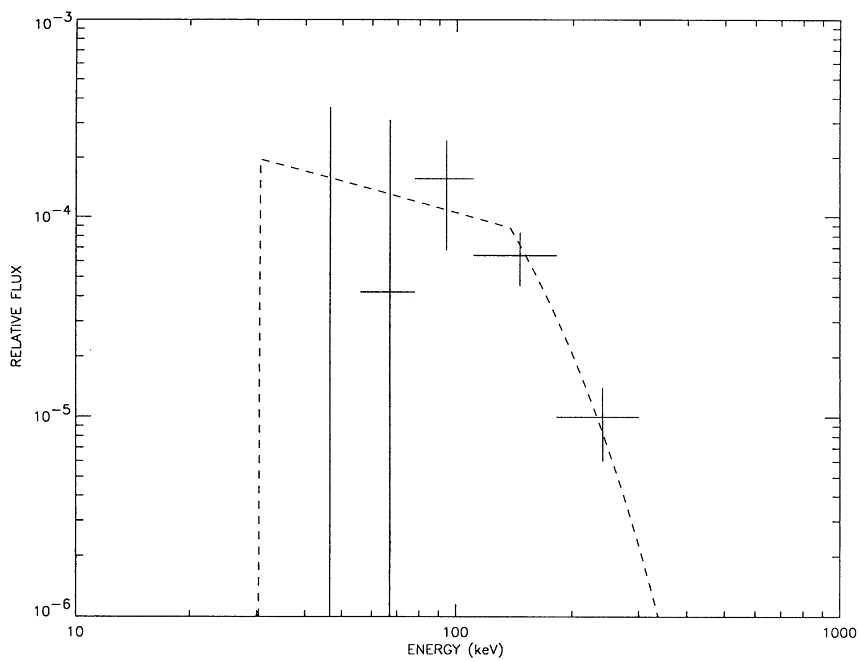

FIG. 6.—Comparison of our derived runaway electron distribution (*dashed line*) with the inverted distribution of Johns & Lin (1992; data points) for the first spike ($t = 85$) in the 1980 June 27 event.

spike emission, even with high time resolution data. This confirms that the two components are physically distinct, since if a spike were an enhancement of the gradual component, the subtraction would not be necessary. Again, if the gradual component at $t = 5$ and 35 is used for the earliest spike in the 1980 June 27 event, the resulting spike spectrum is difficult to interpret in terms of runaway acceleration and Joule heating. However, if a separate gradual component is assumed early in the flare (using $t = 5$ and 15), the resulting spectrum lends itself readily to interpretation. To sum up, since this model assumes that only simple electric field acceleration and heating occurs in the flare, we are led to the conclusion that the gradual and spike components are physically distinct.

Our conclusion that the X-ray emission can be obtained with classical resistivity implies that the heating and acceleration necessarily occur in many current/return current channels, whether sheets or filaments, and this is consistent with our findings. Type III radio observations of this hard X-ray burst show strong evidence that such fragmentation of the acceleration region did indeed occur (Aschwanden et al. 1990).

The idea of large numbers of fine-scale currents is not new (Hoyng 1977; Spicer 1983; Holman 1985; Tsuneta 1985; Winglee et al. 1991). The observation that s varies systematically by two orders of magnitude is suggestive, and may tell us something fundamental about the flare process. It is consistent with the notion that a flare is an avalanche of many small-scale energy-release events (Lu & Hamilton 1991). If the currents are aligned along a flux tube, an immediate consequence is that electrons would be accelerated in both directions along the length of the loop, and thick-target emission would be observed at both footpoints. This is frequently seen with the Hard X-ray Telescope on board the *Yohkoh* satellite (Kosugi et al. 1992; Sakao et al. 1992). The observed area of the emission is then the integrated sum of all of the fine-scale currents' emissions.

Such highly fragmented, oppositely directed fine-scale current structures are observed in the Earth's auroral zone (e.g., Fukunishi et al. 1991). It is tempting to draw analogies from these in arguing in favor of DC electric field acceleration in solar flares (e.g., Lin & Schwartz 1987; Johns & Lin 1992), but the particle "injection" methods may be different. For the Earth, the electrons are introduced into the currents via flux transfer events, and are thus accelerated en masse from one end of a current sheet to the other. When observed, the entire group will have similar energies, producing a peak in the distribution. This could of course also be possible in the solar case. Equally probable, however, is that electrons are uniformly "injected" along the length of a current sheet, by being either scattered up in energy from the thermal current or swept into the current sheet from the sides. This means there is no unique energy to which all of the electrons are accelerated. Rather, they are continually spread out in energy from a minimum ($\mathscr{E}_{cr}$) to a maximum ($\mathscr{E}_{co}$) value. The energy gain of an individual electron is determined by the fraction of the total potential drop over which it is accelerated. The range of energy gains produces the runaway plateau to which we have referred. Figure 6 shows that this situation is indeed possible. The same idea has been used to explain some aspects of the time-lag sometimes seen for high-energy photons (Dulk, Kiplinger, & Winglee 1992).

Lin & Johns (1993) have used their inversion technique coupled with a continuity equation to determine the accelerated electrons for the same set of spectra which we have examined. In summing their electrons over energies exceeding our derived $\mathscr{E}_{cr}$, we get these values of accelerated electrons s^{-1} (to be compared with Table 1): $t = 15$, 1.3×10^{33}; $t = 35$, 1.1×10^{33}; $t = 60$, 8.9×10^{33}; $t = 100$, 2.9×10^{33}; $t = 125$, 2.4×10^{34}; and $t = 150$, 4.5×10^{33}. It is clear that our results and those of Lin & Johns are in excellent agreement, except at $t = 14$ and 100. The source of the discrepancy is unknown. Their derived energetics for the first spike ($t = 87.5$, 4×10^{34} electrons s^{-1}, 4.8×10^{27} ergs s^{-1}) are larger than ours, but this is expected since they used electrons down to 23 keV while our deduced $\mathscr{E}_{cr}$ is 38.1 keV.

This model has implications for hard X-ray imaging of flares. As mentioned above, if the currents are aligned along a magnetic loop, we expect footpoint emission from the accelerated electrons. We also expect an extended source of thermal emission, due to the gradual component, at the lower hard X-ray energies, reflecting the heated plasma throughout the volume V^{Q}. Being thermal, this emission would fall off at the higher photon energies, allowing footpoint emission to be seen from those electrons accelerated in the gradual component. During strong spikes, additional footpoint emission will be seen, which may or may not be spatially coincident with that seen during the interspike minima, since the two components are physically distinct. Depending on the strength of the spike relative to the gradual component, and the dynamic range of the hard X-ray telescope, the footpoint emission during the spikes may dominate the extended thermal source at all energies. The HXT instrument onboard the *Yohkoh* spacecraft has recorded flares in which a hard spectrum double source is seen during the spikes, and an extended emission (encompassing both parts of the double source) with a soft spectrum is seen during the interspike minima (Sakao et al. 1992). This is consistent with the predictions of this model.

The picture that we are developing is consistent with both microwave and soft X-ray observations. Since runaway-producing currents are either field-aligned or in magnetically neutral sheets, little gyrosynchrotron emission is expected from them. If only a few runaways escape the sheets into the surrounding heated plasma, however, both thermal and nonthermal microwave radiation would result which can account for the observed spectra (Benka & Holman 1992). Alternatively, if the magnetic field is converging the microwave emission could arise from mirroring electrons as suggested by Benka & Holman (1992).

Finally, since the currents continually heat the coronal plasma, and accelerate far fewer electrons than in the 100% nonthermal beam model, this may account for the observed large stationary component with blue-wing enhancements seen in Ca XIX early in many flares. The nonthermal beam model predicts ubiquitous blueshifts of the entire line (Li, Emslie, & Mariska 1989), which are not observed. The reduced number of precipitating electrons in our model would also reduce the amount of (blueshifted) material evaporated from the chromosphere, while the thermal emission would always provide a stationary component to the emission. Late in the flare, other authors have found that a continued energy input is often required, even after the impulsive hard X-ray burst is over (Dennis & Zarro 1993). This is consistent with the persistence of Joule heating in the flare plasma even when the runaways are not of great importance to the energetics. The falling value of ϵ also indicates that acceleration is becoming less important. When $\epsilon < (kT/mc^2)$ (cf. § 2.1) no runaways are produced and the sole effect of the current is a slow heating.

To sum up, we have presented a self-consistent framework for analyzing hard X-ray emission from solar flares in terms of runaway electron acceleration and Joule heating from DC electric fields, and have analyzed one event in detail. We have found that classical resistivity and sub-Dreicer fields can account for the emission from this event. We have confirmed the hypothesis of Lin & Schwartz that there are two distinct components of the hard X-ray emission in this event, and found a signature of runaway acceleration in the spectral hardness of the emission from the spike component. Plasma heating is seen only in the gradual component. We have shown that physical information can be reliably obtained from high-resolution hard X-ray spectra. We look forward to combining such spectrally derived information with high spatial resolution hard X-ray imaging, such as can be provided by NASA's High-Energy Solar Physics (HESP) mission.

We thank Richard Schwartz for providing the X-ray spectra analyzed here. We also thank Bob Lin and Chris Johns for sharing their results with us prior to publication. We had many useful discussions with Brian Dennis, Bob Lin, Peter MacNeice, Spiro Antiochos, and John Mariska. We also received a number of helpful comments from an anonymous referee. This work was done while S. G. B. was a National Academy of Sciences/NRC Research Associate at the Naval Research Laboratory.

REFERENCES

Aschwanden, M. J., Benz, A. O., Schwartz, R. A., Lin, R. P., Pelling, R. M., & Stehling, W. 1990, Sol. Phys., 130, 39
Benka, S. G., & Holman, G. D. 1992, ApJ, 391, 854
Böhme, A., Fürstenberg, F., Hildebrandt, J., Saal, O., Krüger, A., Hoyng, P., & Stevens, G. A. 1977, Sol. Phys., 53, 139
Brown, J. C. 1971, Sol. Phys., 18, 489
Cohen, R. H. 1976, Phys. Fluids, 19, 239
Connor, J. W., & Hastie, R. J. 1975, Nucl. Fusion, 15, 415
Crannell, C. J., Frost, K. J., Mätzler, C., Ohki, K., & Saba, J. L. 1978, ApJ, 223, 620
de Groot, S. R., van Leeuwen, W. A., & van Weert, ChG. 1980, Relativistic Kinetic Theory (Amsterdam: North-Holland)
Dennis, B. R. 1988, Sol. Phys., 118, 49
Dennis, B. R., & Schwartz, R. A. 1989, Sol. Phys., 121, 75
Dennis, B. R., & Zarro, D. M. 1993, Solar Phys., 146, 177
Dreicer, H. 1959, Phys. Rev., 115, 238
Dulk, G. A., Kiplinger, A. L., & Winglee, R. M. 1992, ApJ, 389, 756
Emslie, A. G., Coffey, V. N., & Schwartz, R. A. 1989, Sol. Phys., 122, 313
Fuchs, V., Cairns, R. A., & Lashmore-Davies, C. N. 1986, Phys. Fluids, 29, 2931
Fuchs, V., Shoucri, M., & Teichmann, J. 1988, Phys. Fluids, 31, 2221
Fukunishi, H., Fujii, R., Kokubun, S., Tohyama, F., Mukai, T., & Oya, H. 1991, Geophys. Res. Lett., 18, 297
Hakim, R. 1967, Phys. Rev., 162, 128
Hamilton, R. J., & Petrosian, V. 1992, ApJ, 398, 350
Heyvaerts, J. 1981, in Solar Flare Magnetohydrodynamics, ed. E. R. Priest (New York: Gordon & Breach)
Holman, G. D. 1985, ApJ, 293, 584
Holman, G. D., & Benka, S. G. 1992, ApJ, 400, L79
Holman, G. D., Kundu, M. R., & Kane, S. R. 1989, ApJ, 345, 1050
Hoyng, P. 1977, A&A, 55, 23
Johns, C. M., & Lin, R. P. 1992, Sol. Phys., 137, 121
Kosugi, T., et al. 1992, PASJ, 44, L45
Kruskal, M., & Bernstein, I. B. 1962, in Princeton Plasma Physics Laboratory Report No. MATT-Q-20, 174
Kulsrud, R. M., Sun, Y-C., Winsor, N. K., & Fallon, H. A. 1973, Phys. Rev. Lett., 31, 690
Li, P., & Emslie, A. G. 1990, Sol. Phys., 129, 113
Li, P., Emslie, A. G., & Mariska, J. T. 1989, ApJ, 341, 1075
Lin, R. P., & Hudson, H. S. 1976, Sol. Phys., 50, 153
Lin, R. P., & Johns, C. M. 1993, ApJ, 417, L53
Lin, R. P., & Schwartz, R. A. 1987, ApJ, 312, 462
Lin, R. P., Schwartz, R. A., Pelling, R. M., & Hurley, K. C. 1981, ApJ, 251, L109
Lu, E. T., & Hamilton, R. J. 1991, ApJ, 380, L89
Meyer, J.-P. 1985, ApJS, 57, 173
Nitta, N., Kiplinger, A. L., & Kai, K. 1989, ApJ, 337, 1003
Sakao, T., et al. 1992, PASJ, 44, L83
Schwartz, R. A., Fishman, G., Meegan, C., Wilson, R., & Paciesas, W. 1993, Adv. Sp. Res., 13, (9), 233
Shevgaonkar, R. K., & Kundu, M. R. 1985, ApJ, 292, 733
Singh, N. 1977, Phys. Lett., 63A, 307
Somov, B. V. 1992, Physical Processes in Solar Flares (Dordrecht: Kluwer)
Spicer, D. S. 1982, Sp. Sci. Rev., 31, 351
———. 1983, Adv. Sp. Res., 2, No. 11, 135
Spitzer, L., & Härm, R. 1953, Phys. Rev., 89, 977
Tandberg-Hanssen, E., & Emslie, A. G. 1988, The Physics of Solar Flares (Cambridge: Cambridge Univ. Press)
Tsuneta, S. 1985, ApJ, 290, 353
Tucker, W. H. 1975, Radiation Processes in Astrophysics (Cambridge: MIT Press)
Wiley, J. C., & Hinton, F. L. 1980, Phys. Fluids, 23, 921
Wilkinson, L. K., Emslie, A. G., & Gary, G. A. 1992, ApJ, 392, L39
Willson, R. F., Klein, K.-L., Kerdraon, A., Lang, K. R., & Trottet, G. 1990, ApJ, 357, 662
Willson, R. F., Lang, K. R., & Gary, D. E. 1993, ApJ, 418, 490
Winglee, R. M., G. A., Bornmann, P. L., & Brown, J. C. 1991, ApJ, 375, 382